

## New Constraints on Neutron Star Cooling from *Chandra* Observations of 3C58

Patrick Slane<sup>1</sup>, David J. Helfand<sup>2</sup>, and Stephen S. Murray<sup>1</sup>

### ABSTRACT

3C58 is a young Crab-like supernova remnant. Historical evidence strongly suggests an association of the remnant with supernova SN 1181, which would make 3C58 younger than the Crab Nebula. Recent *Chandra* observations have identified the young 65 ms pulsar J0205+6449 at its center, embedded in a compact nebula which, we show here, appears to be confined by the pulsar wind termination shock. We present new *Chandra* observations of this compact nebula and embedded pulsar which set strong upper limits on thermal emission originating from the neutron star surface. These limits fall far below predictions of standard neutron star cooling, requiring the presence of exotic cooling processes in the neutron star core.

*Subject headings:* ISM: individual (3C58), pulsars: individual (PSR J0205+6449), stars: neutron, supernova remnants, X-rays: general

### 1. Introduction

Neutron stars are macroscopic manifestations of processes that otherwise occur only in individual atomic nuclei. Formed hot in the core collapse that terminates the life of a massive star, they are supported against gravitational implosion by neutron degeneracy pressure. However, details of the interior structure of neutron stars (NSs) remain poorly understood, largely due to our incomplete understanding of the strong interaction at ultrahigh densities. In the early stages of their lives, energy loss is dominated by neutrino emission. However, the neutrino production rate is highly dependent upon the structure of the interior. In the

---

<sup>1</sup>Harvard-Smithsonian Center for Astrophysics, 60 Garden Street, Cambridge, MA 02138

<sup>2</sup>Department of Astronomy, Columbia University

“normal” cooling scenario, neutrino production proceeds via the modified URCA process, neutrino bremsstrahlung in the stellar crust, and plasmon decay. The residual heat diffuses from the core to the surface, manifesting itself as blackbody-like emission (modified by effects of any residual atmosphere) which peaks in the soft X-ray band. The rate at which the surface temperature declines depends critically upon the neutrino emission rate, and thus provides constraints on hadronic physics at high densities.

In some models, the energy density of nucleons in the core is sufficiently high that the production of pion or kaon condensates, or quark matter, are predicted. The presence of such exotic particles enhances the neutrino rate immensely, resulting in much more rapid cooling. Consequently, measurements of the surface temperature for NSs of known age can provide important constraints on NS interiors, and thus on our knowledge of the strong interaction. Here we present observations of 3C58, a young Crab-like nebula believed to be associated with the supernova of 1181 AD. Given this age, 3C58 is presumably powered by one of the youngest neutron stars in the Galaxy, and one for which the residual cooling emission should be measurable if standard cooling models apply – a prospect that has motivated many searches for the pulsar and its cooling emission. The pulsar in 3C58 was recently discovered by Murray et al. (2002). To date, however, the strongest upper limit on cooling from the NS surface yielded a value well in excess of standard cooling curves (Helfand et al. 1995), while Torii et al. (2000) reported hot blackbody emission associated with a small emitting area that they associated with hot polar caps - a result inconsistent with *XMM* studies by Bocchino et al. (2001). Here we present *Chandra* observations and modeling of the emission from the NS which yield a surface temperature well below that predicted by standard cooling curves, providing strong support for the presence of enhanced neutrino production rates in the stellar interior.

## 2. Observations

3C 58 was observed with the ACIS detector onboard the *Chandra* Observatory on 04 September 2000. The aimpoint was placed on the S3 chip of the detector, and a 1/2-subarray mode was selected in order to minimize pileup from the compact central source while still imaging most of the pulsar wind nebula (PWN). Standard cleaning of the data to remove episodes of high background resulted in a final exposure of 33.8 ks. The image clearly reveals a compact central core, as reported by Murray et al. (2001) based on *Chandra* HRC observations, as well as other apparent structure in the inner nebula – most notably an arc of emission apparently emanating from the central region (Figure 1).

A total of eight relatively bright point sources are observed in the field defined by the

S3 and S4 ACIS chips. Based on identification of stellar counterparts for four of these, we obtained a position reconstruction error of  $\Delta\text{RA} = -0.17 \pm 0.12$  arcsec and  $\Delta\text{Dec} = +0.64 \pm 0.08$  arcsec, within typical accuracies for *Chandra* positions.

### 3. Data Analysis

#### 3.1. Spatial Modeling

The central region of 3C58 is shown in Figure 2. The emission is clearly extended, with elongation in the N-S direction, perpendicular to the long axis of the main nebula. The pulsar PSR J0205+6449 (Murray et al. 2001) resides at the center of this compact nebula. We have carried out spatial modeling of the emission using a three-component model consisting of a 2-D gaussian combined with a point source, both superposed on a flat background. For the point source, we used a model of the *Chandra*-ACIS point spread function for the mean position of the central region. The free parameters in the fit are the central position, widths, rotation angle, and normalization of the 2-D gaussian, the position and normalization of the PSF model, and the surface brightness of the background. Our best-fit parameters for the 2-D gaussian yield a FWHM (along the long axis) of  $4.2'' \pm 0.04''$  and an ellipticity of  $0.49 \pm 0.01$ , with the long axis running almost exactly north-south. In fact, Figure 2 shows that the full extent of the elongated core is  $\sim 25''$  in the N-S direction. Murray et al. (2002) find similar results using HRC data, though a somewhat smaller extent which may be the result of the factor of  $\sim 2.5$  fewer counts in the HRC image, as well as the fact that the 2-D gaussian model is only a rough approximation of the more extended structure. The best-fit point source location, when corrected for the offsets described above, is  $\text{RA}_{2000}: 02^{\text{h}}05^{\text{m}}37.92^{\text{s}}$ ,  $\text{Dec}_{2000}: +64^{\circ}49'42.8''$ ; the total number of counts from this component is  $880 \pm 78$  (90% confidence).

The western edge of the core nebula lies directly along a radio filament (Frail & Moffett 1993), shown as contours in Figure 2, and there appears to be a slight flattening of nebula along this side. Frail & Moffett (1993) suggested that this filament may represent the position of the termination shock where the pulsar wind is confined by the interior pressure of the PWN. Adopting the generally accepted distance  $d = 3.2d_{3.2}$  kpc (see Section 4.1), integration of the radio synchrotron spectrum yields a pressure of  $P_{\text{neb}} = 3.2 \times 10^{-10} d_{3.2}^{-1}$  dyne  $\text{cm}^{-2}$  under the assumption of equipartition between the electron and magnetic energy densities. The ram pressure of the pulsar wind  $P_{\text{wind}} = \dot{E}/4\pi\eta cr_w^2$ , where the wind covers a fraction  $\eta$  of a sphere,  $\dot{E}$  is the energy loss rate of the pulsar, and  $r_w$  is the distance from the pulsar at which wind confinement occurs. The spin-down properties of the pulsar give  $\dot{E} = 2.6 \times 10^{37} I_{45}$  erg  $\text{s}^{-1}$  (Murray et al. 2001) where  $I_{45}$  is the NS moment of inertia in

units of  $10^{45}$  gm cm<sup>2</sup>. Pressure balance should thus occur at  $r_w = 5.5 \times 10^{17} I_{45}^{1/2} \eta^{-1/2} d_{3.2}^{1/2}$  cm, or at an angular distance  $\theta = 11.4 I_{45}^{1/2} \eta^{-1/2} d_{3.2}^{-1/2}$  arcsec. This is in good agreement with the the  $\sim 12$  arcsec radial extent of the core X-ray emission in the NS direction, suggesting that the compact nebula surrounding the pulsar is bounded by the pulsar wind termination shock. It is possible that this is actually a toroidal structure, much like that seen in the Crab Nebula, and that the elongated surface brightness distribution is the result of the inclination angle. In this interpretation, the axis of the toroid, which presumably lies along the rotation axis of the pulsar, lies in the east-west direction when projected onto the sky. We note that the long axis of 3C58 itself, as well as an extended jet-like feature shown in Figure 2, are both aligned in this direction. Assuming that the radio filament lies along one side of the torus, its separation from the pulsar ( $\sim 4.5$  arcsec) implies an inclination angle of  $\sim 70^\circ$ . We defer detailed discussion of this picture, including the jet-like feature in Figure 2 and other possible outflow-related structures seen in Figure 1, to a future publication.

### 3.2. Spectral Modeling

Previous measurements of the column density for 3C58 yield  $N_H = (3.3 \pm 0.4) \times 10^{21}$  cm<sup>-2</sup> (Torii et al. 2000). This is consistent with values reported by Bocchino et al. (2001). Using the entire nebula, and allowing the photon index to vary with radius<sup>3</sup> we obtain  $N_H = (3.75 \pm 0.11) \times 10^{21}$  cm<sup>-2</sup>. Using this value, the spectrum from the central  $3 \times 3$  pixel region<sup>4</sup> in 3C58 is well fit ( $\chi_r^2 = 0.82$ ) by an absorbed power law with a photon index  $\Gamma = 1.73 \pm 0.07$  (Figure 3); blackbody or thermal plasma models are ruled out at high significance. In particular, contrary to results from ASCA studies (Torii et al. 2000), we find no evidence of a soft blackbody component from the central source, which is consistent with the results of Bocchino et al. (2001). The majority of equations of state yield an effective NS radius larger than 12 km for any range of masses (Haensel 2001). To establish an upper limit to the effective blackbody temperature of any such a component, we have fixed the column density at the upper end of the 90% confidence interval quoted above, added a blackbody model with  $R_\infty = 12$  km to the power law, and varied the temperature of this component until the spectral fit probability fell to  $10^{-4}$ . In re-fitting the data, we allowed the power law index to vary as well. The upper limit we determine is  $T_\infty < 1.08 \times 10^6$  K. The model containing this thermal component is shown in Figure 3, and clearly exceeds what can be

---

<sup>3</sup>A variation in spectral index with radius is expected from synchrotron cooling. These results will be presented in a future publication.

<sup>4</sup>Each ACIS pixel is 0.492 arcsec on a side.

accommodated in the data. For comparison, we also plot the expected flux for a blackbody component whose temperature is that expected from standard neutron star cooling curves.

As with all stars, the emission from the surface of a NS is not a blackbody; rather, it is modified by the presence of whatever atmosphere might exist. One expects the surface of the NS to be covered with Fe, but an atmosphere consisting of H, He, and/or intermediate-mass elements acquired either from ejecta fallback following the neutron star’s formation, or from material accreted from the ISM, is also a possibility. From models of nonmagnetic atmospheres, the primary effect of H or He atmospheres is a considerable deviation of the high energy end of the spectrum relative to the Wien tail of a pure blackbody. The result is that the best-fit blackbody model overestimates the effective temperature – typically by as much as a factor of two. For atmospheres dominated by heavier elements the blackbody fit gives a good approximation to the temperature (Lloyd, Hernquist, & Heyl 2002). The temperature upper limit derived above is thus conservative.

### 3.3. Spatial/Temporal Modeling

The temporal information from PSR J0205+6449 provides an additional constraint on any thermal emission originating at the surface of the NS. The spectral results summarized above clearly establish that the bulk of the flux from the pulsar is nonthermal. The narrow pulse profile measured by Murray et al. (2001) is consistent with this picture. While temperature nonuniformities on the NS surface can, in principle, lead to a pulsed X-ray signal, light bending effects from the strong gravitational field result in considerable broadening of any such pulse profile (Yancopoulos, Hamilton & Helfand 1994; Zavlin, Shibano & Pavlov 1995) The very sharp pulse profile of PSR J0205+6449 is inconsistent with such an origin. We can thus use the strength of the pulsed signal along with the modeled brightness of the pointlike component to obtain an independent limit on any remaining emission arising from surface cooling.

In the 33 ks HRC-S observation of 3C58, the pulse profile for PSR J0205+6449 yields a total of  $\sim 127.2 \pm 17.2$  counts (90% confidence) above the mean flux level in the narrow phase bins containing the bulk of the pulsed power. The count rate conversion between ACIS-S and HRC-S based on the measured power law spectrum reported above is  $R_{\text{HRC-S}} = 0.26 R_{\text{ACIS-S}}$ . The lower limit to the number of pulsed counts in the  $\sim 34$  ks ACIS-S observation is thus  $\sim 435$ . Our spatial modeling yields a total of  $880 \pm 78$  counts from the point source in ACIS-S. The 90% confidence upper limit to the number of unpulsed counts is thus  $\sim 523$ , for an ACIS-S count rate of  $1.54 \times 10^{-2}$  ct s $^{-1}$ . For a radius at infinity of 12 km, the upper limit to the blackbody temperature is  $1.13 \times 10^6$  K, consistent with the limit obtained through

spectral modeling. As we discuss below (and show in Figure 4), this limit falls well below values predicted for standard cooling models assuming the historical age of 3C58. We note that the limit depends on uncertainties in the distance and column density. However, even at the most extreme values of acceptable column density based on fits to the entire nebula, the distance required to match the standard cooling predictions is  $\sim 6$  kpc, a value inconsistent with that inferred from HI measurements.

## 4. Discussion

Our measurement of an upper limit to the temperature of the young NS in 3C58 provides the strongest constraint on NS cooling yet derived, and poses significant problems for standard cooling models. We explore here the implications of our result for the nuclear equation of state and the structure and evolution of NS.

### 4.1. Neutron Star Cooling

The cooling rate of isolated NSs has been a subject of considerable theoretical work predating even the discovery of the first pulsars (e.g. Bahcall & Wolf 1965a,b). The poorly understood properties of the strong nuclear potential at the densities found in NS interiors make these calculations difficult, and lead to a wide range of predictions based on different assumptions for the equation of state, composition, and details of superconductivity (see, e.g., the review by Tsuruta 1998, and references therein). While there is a clear consensus that the early cooling proceeds via neutrino emission from the NS core, the time scale over which this dominates depends critically on the neutrino production rate which, in turn, can vary by orders of magnitude depending upon the state of matter in the interior.

Broadly speaking, models can be divided into “standard” and “non-standard” cooling scenarios. The former class is based upon neutrino emission via the modified URCA process, n–n and p–p neutrino bremsstrahlung, crust neutrino bremsstrahlung, and plasmon neutrino processes. Assumptions must still be made in the cooling calculations, such as the form of the nucleon-nucleon force and the many-body technique used to determine the equation of state, but the differences between stiff and soft equations of state are not large for this class of models. In Figure 4, we plot a variety of cooling curves associated with different models for the NS interior and its properties (see Page 1998 and references therein)<sup>5</sup>. The solid

---

<sup>5</sup>Tabulated values are available at <http://www.astroscu.unam.mx/neutrones/NS-Cooler/NS-Cooler.html>

curve corresponds to “standard” cooling using an equation of state of moderate stiffness.

Non-standard cooling models incorporate neutrino emissivities associated with other processes that may operate in NS interiors. These include the presence of pion condensates which may form at sufficiently high densities. The resulting pion-induced beta decay leads to very a high neutrino emissivity and a correspondingly shorter cooling time for the NS interior (Bahcall & Wolf 1965a,b, Maxwell et al. 1977). Similar processes involving kaon condensates or quark matter may operate as well. Alternatively, strong magnetic field effects in the crust may allow the normal URCA process to proceed, which also leads to extremely high neutrino production rates. These exotic cooling mechanisms modify the NS cooling curves substantially. The dashed curves in Figure 4 represent approximations for several nonstandard cooling models to illustrate the associated rapid cooling (Page 1998). The effects of superfluidity can substantially moderate the rapid cooling because the significantly reduced heat capacity of the superfluid particles reduces the neutrino rate considerably.

We have indicated on Figure 4 the upper limit for surface cooling emission from PSR J0205+6449 derived above. It is evident that the limit falls considerably below predictions from standard cooling models, suggesting the presence of some exotic cooling contribution in the interior. We note that the placement of this point on the cooling curves depends upon the age assumption for 3C58. Here we have used the historical age based on association with SN 1181. Four independent written records – two from Japan, and one each from the northern and southern Chinese empires – record the presence of a guest star that appeared in the late summer of AD 1181 and was visible to the naked eye for nearly 6 months. Detailed analysis of the star’s celestial coordinates are summarized by Stephenson and Green (1999) who identify a faint star near  $\epsilon$  Cas as the closest permanent star to the location of the event. This position lies less than  $2^\circ$  from 3C58. The only other young supernova remnant within  $10^\circ$  is Tycho’s SNR, the unambiguously identified remnant of SN 1572. The association of 3C58 with SN 1181 thus appears extremely secure. However, even if we increase the age estimate to 5000 yr, as has been suggested based on optical and radio expansion data (Fesen 1985, Bietenholz et al. 2001), the measurement still falls below standard cooling models (see Figure 4). Deeper high-resolution X-ray measurements of 3C58 are of considerable interest in order to further constrain this important diagnostic of the NS interior.

## 5. Summary

The size of the extended emission region immediately surrounding the pulsar in 3C58 is consistent with that expected for the termination shock where the pulsar wind pressure is balanced by the interior pressure of the nebula. The elongated morphology, along with the

position and size of an apparently associated radio filament, suggest a toroidal morphology similar to that observed in the Crab Nebula. The orientation of the torus suggests a pulsar rotation axis aligned in the east-west direction, along the primary axis of extension of 3C58 itself. The inclination angle of the torus is large, and the resulting projected X-ray morphology does not permit us to resolve the toroidal structure with the current X-ray data.

Our *Chandra* observations of 3C58 and its associated pulsar provide important constraints on models for NS cooling. The upper limit to the thermal emission from the NS surface falls well below predictions from standard cooling models and appears to require the presence of some rapid cooling mechanism. Additional time-resolved observations of the pulsar could further constrain this limit, providing important new information on the equation of state of nuclear matter and the structure of NS interiors.

The authors would like to thank John Bahcall for helpful discussions on NS cooling and Dale Frail for supplying the VLA image of the central region in 3C58. We also thank Bryan Gaensler for his helpful suggestions and careful reading of the text. This work was supported in part by the National Aeronautics and Space Administration through contract NAS8-39073 and grant GO0-1117A (POS) and contract NAS8-38248 (SSM).

## REFERENCES

- Bahcall, J. N., & Wolf, R. A. 1965a, *ApJ*, 142, 1254
- Bahcall, J. N., & Wolf, R. A. 1965b, *PhRvL*, 14, 343
- Bietenholz, M. F., Kassim, N. E., & Weiler, K. W. 2001, *ApJ*, 560, 772
- Bocchino, F., Warwick, R. S., Marty, P., Lumb, D., Becker, W., & Pigot, C. 2001, *A&A*, 369, 1078
- Fesen, R. A. 1983, *ApJ*, 270, L53
- Frail, D. A. & Moffett, D. A. 1993, *ApJ*, 408, 637
- Gaensler, B. M., Brazier, K. T. S., Manchester, R. N., Johnston, S., & Green, A. J. 1999, *MNRAS*, 305, 724
- Haensel, P. 2001, *A&A* 380, 186
- Helfand, D. J., Becker, R. H., & White, R. L. 1995, *ApJ*, 453, 741
- Kaspi, V. M., Roberts, M. E., Vasisht, G., Gotthelf, E. V., Pivovarov, M., & Kawai, N. 2001, *ApJ*, 560, 371



- Lloyd, D. A., Hernquist, L., & Heyl, J. S. 2002, to appear in “Neutron Stars in Supernova Remnants” (ASP Conference Proceedings), eds P. O. Slane and B. M. Gaensler
- Maxwell, O., Brown, G. E., Campbell, D. K., Dashen, R. F., & Manassah, J. T. 1977, *ApJ*, 216, 77
- Murray, S. S., Slane, P. O., Seward, F. D., Ransom, S. M., & Gaensler, B. M. 2001, *ApJ*-accepted
- Page, D. 1998, in “The Many Faces of Neutron Stars.” Eds. R. Buccheri, J. van Paradijs, & M. A. Alpar. Dordrecht ; Boston : Kluwer Academic Publishers, 1998., p.539
- Roberts, D. A., Goss, W. M., Kalberla, P. M. W., Herbstmeier, U., & Schwarz, U. J. 1993, *A&A*, 274, 427
- Sedov, L. I. 1959, *Similarity and Dimensional Methods in Mechanics* (New York: Academic Press)
- Slane, P., Chen, Y., Schulz, N. S., Seward, F. D., Hughes, J. P. & Gaensler, B. M. 2000, *ApJ*, 533, L29
- Stephenson, F. R. & Green, D. A. 1999, *A&G*, 40b, 27
- Torii, K., Slane, P. O., Kinigasa, K., Hashimoto, K. & Tsunemi, H. 2000, *PASJ*, 52, 875
- Torii, K., Tsunemi, H., Dotani, T., & Mitsuda, K. 1997, *ApJ*, 489, L145
- Tsuruta, S. 1998, *PhR*, 292, 1
- Woltjer, L., Salvati, M., Pacini, F., & Bandiera, R. 1997, *A&A*, 325, 295
- Yancopoulos, S., Hamilton, T. T., & Helfand, D. J. 1994, *ApJ*, 429, 832
- Zavlin, V. E., Shibano, Y. A., Pavlov, G. G. 1995, *AstL*, 21, 149

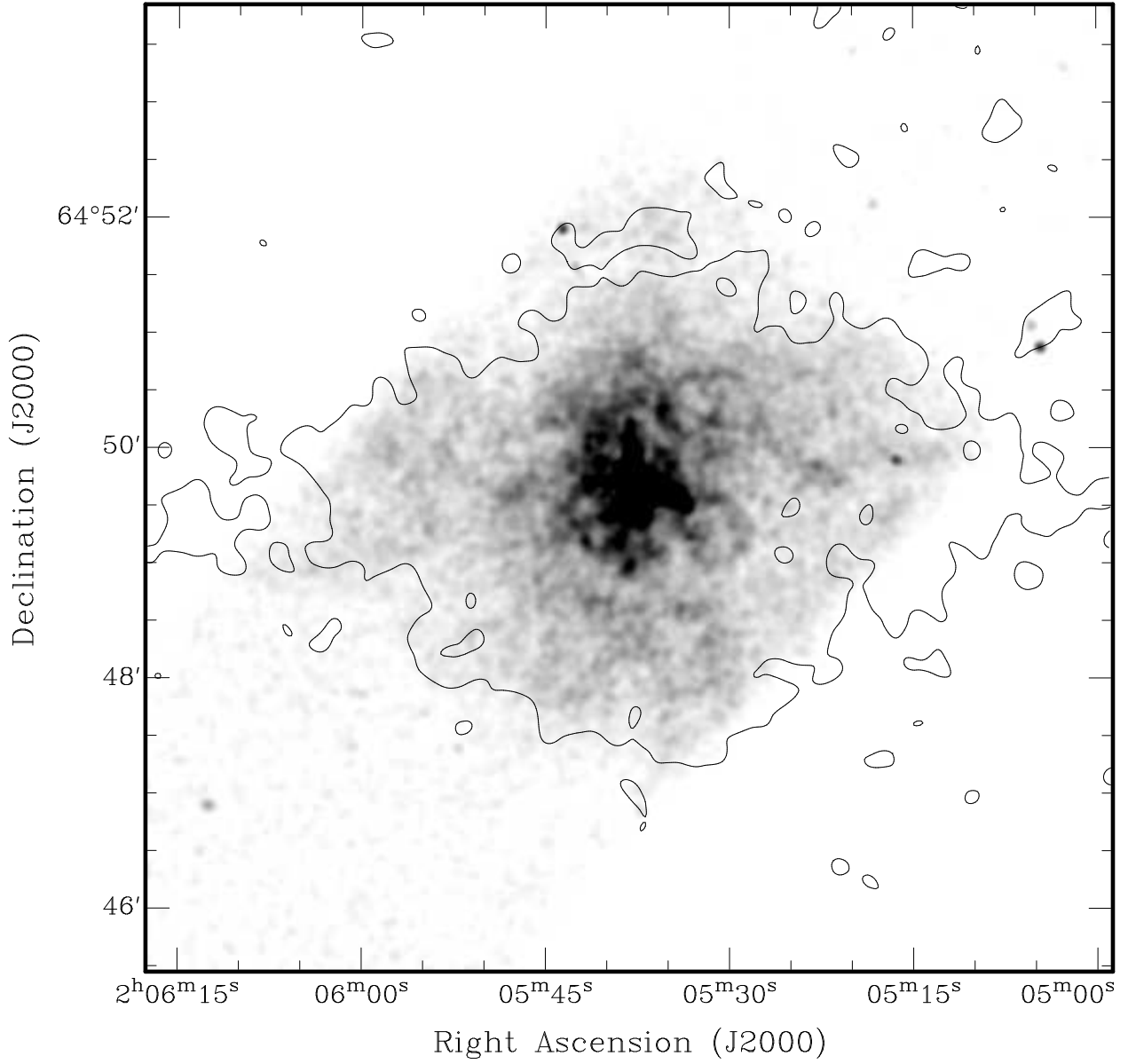


Fig. 1.— ACIS image of 3C58. Some portions of the nebula extend beyond the detector boundary, as indicated by the outermost contour from the HRC image, which is superimposed.

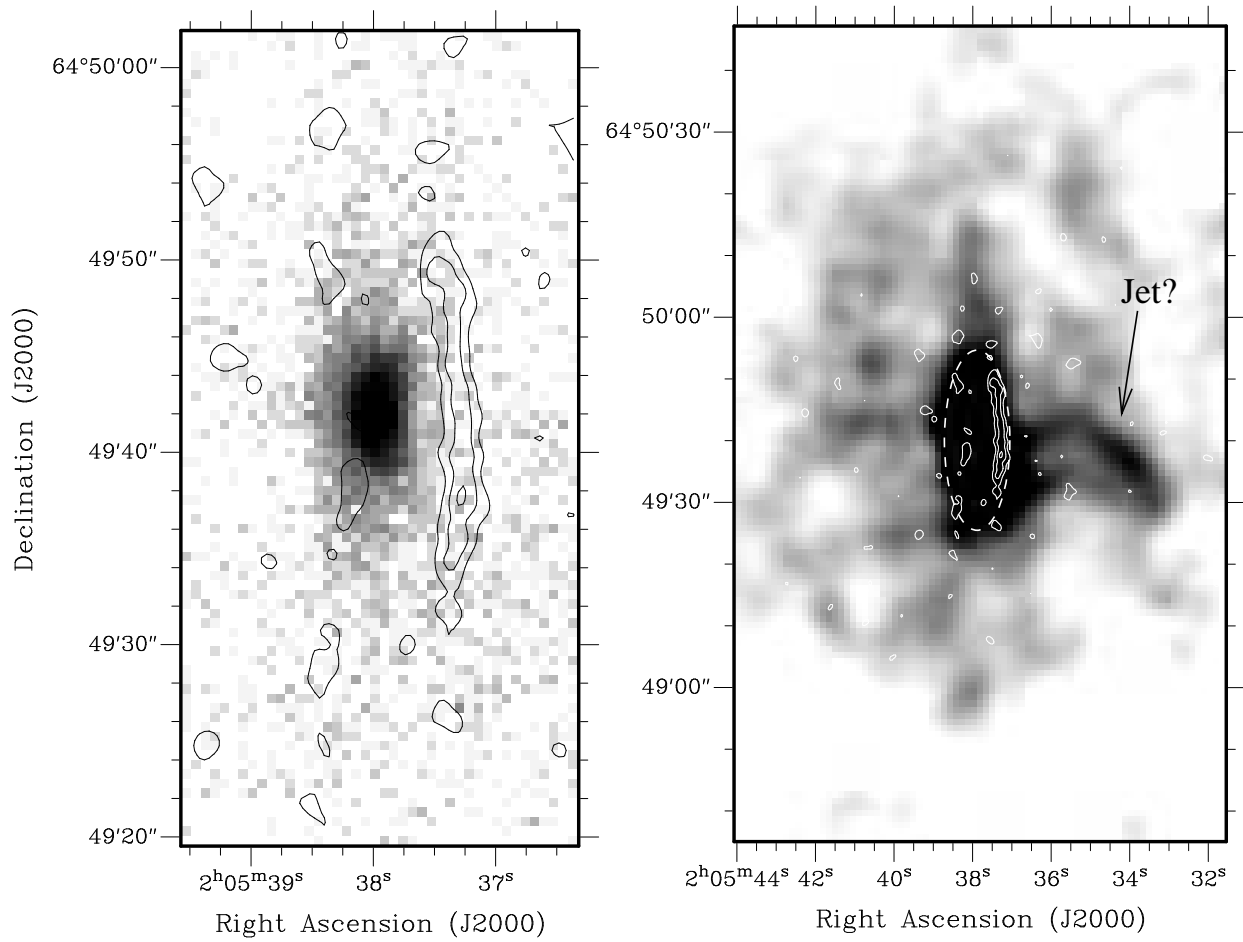


Fig. 2.— **Left:** ACIS image of the central region of 3C58, with contours from 20 cm VLA data showing a faint radio wisp that bounds the X-ray core. **Right:** Saturated image of 3C58 core, on a larger scale, revealing the faint jet-like feature extending toward the west. The dashed ellipse indicates the rough outline of the extended X-ray core.

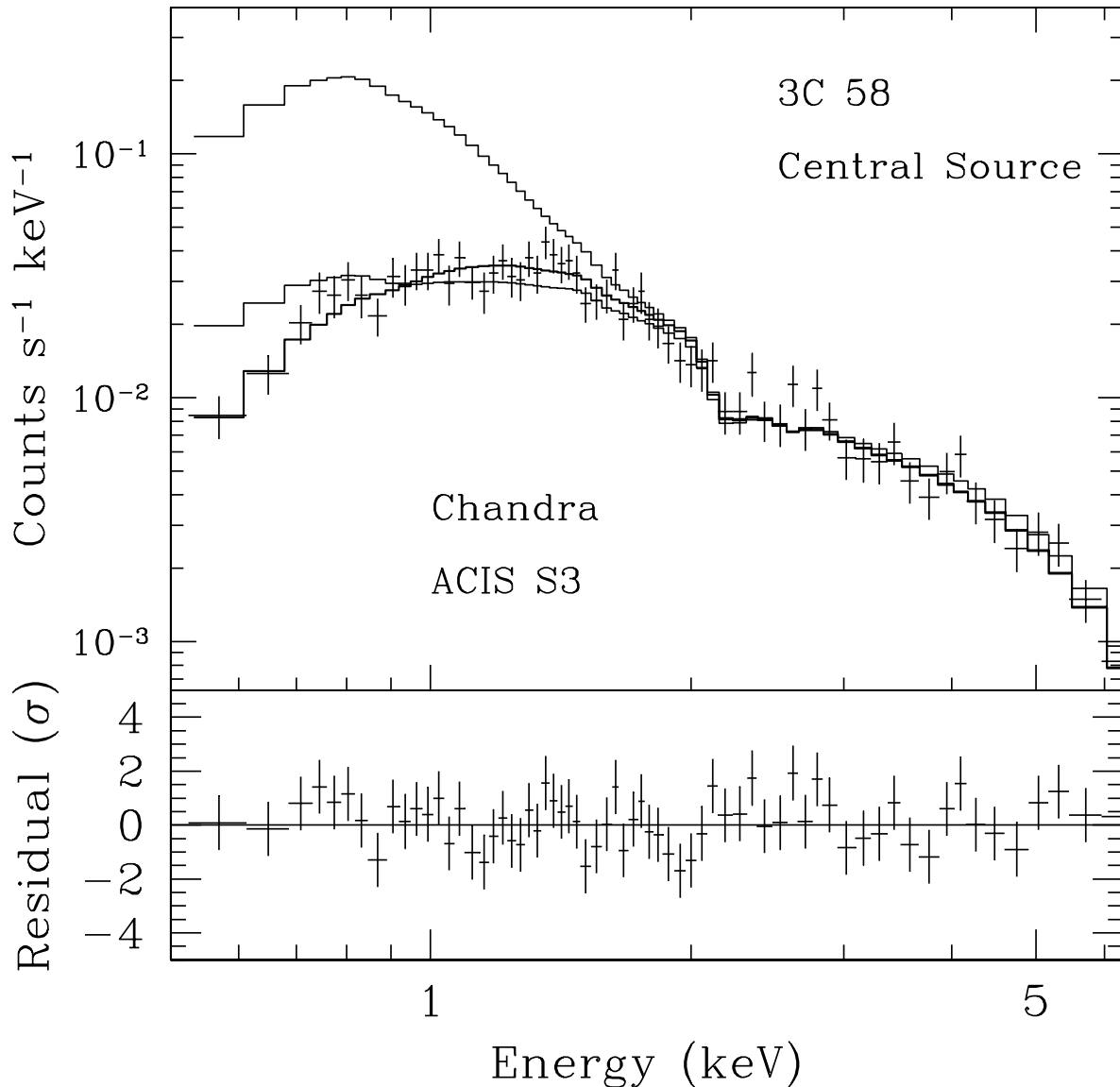


Fig. 3.— ACIS-S spectrum of the central  $3 \times 3$  pixel region ( $1.5'' \times 1.5''$ ) centered on PSR J0205+6449. The lower histogram (matching the data) corresponds to the best-fit power law model. There is no evidence for a soft blackbody-like component. The uppermost histogram depicts a model with an additional component representing blackbody emission from a NS with effective radius 12 km, at a temperature consistent with standard cooling models. The middle histogram (at low energies) corresponds to the same model, but using a temperature determined as the upper limit that could have been present in the 3C58 data.

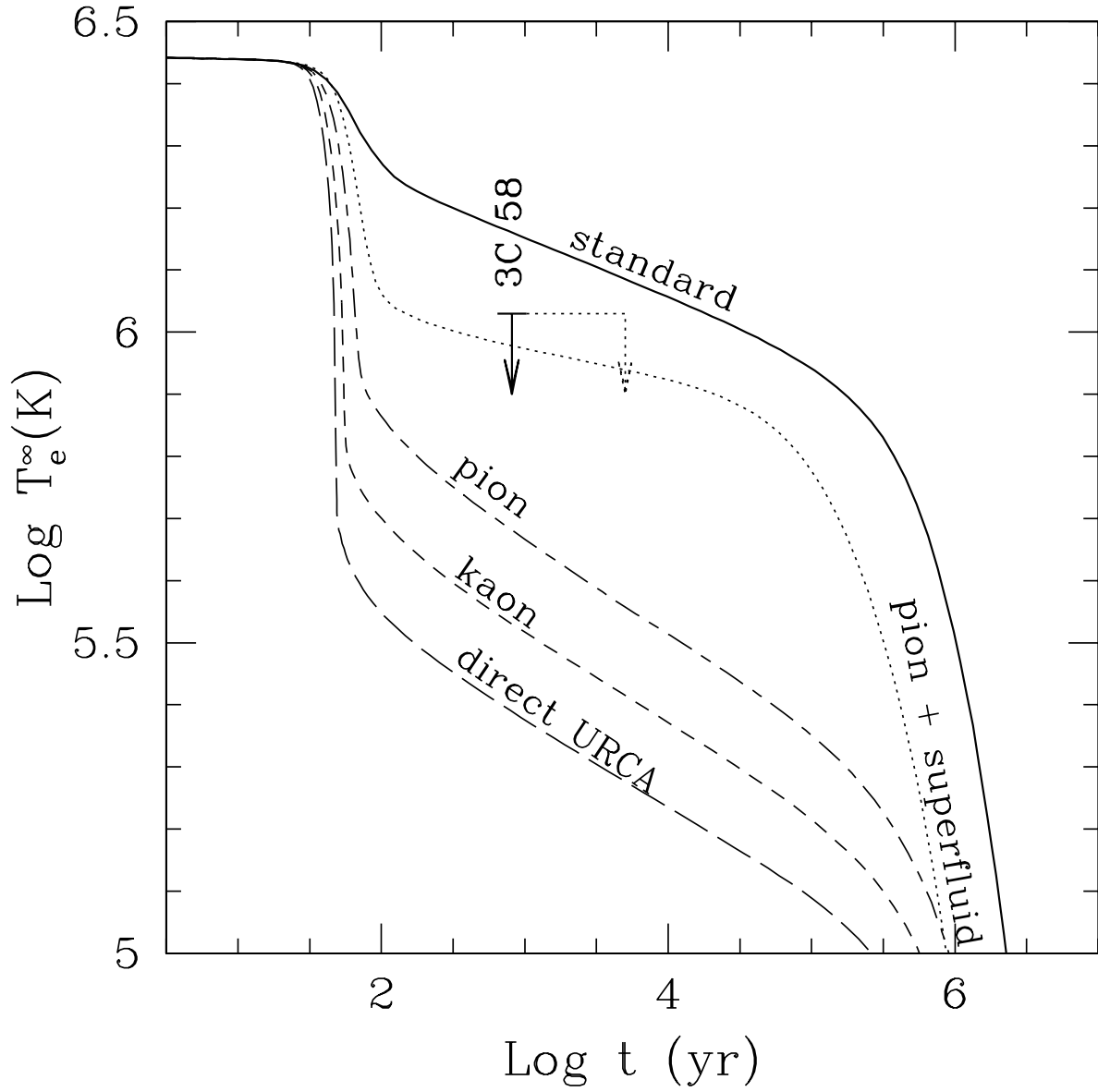


Fig. 4.— Surface temperature upper limit for 3C58, in comparison with predictions for cooling of NS. Model data are from Page 1998. The dashed arrow for 3C58 illustrates the upper limit for the pulsar if the characteristic age, rather than the historical age, is used.